Vietnam Journal of Mechanics, Vol. 47, No. 3 (2025), pp. 208 – 222
DOI: https://doi.org/10.15625/0866-7136/22269

CASCADE CONTROL FOR FEED DRIVE SYSTEMS

Ngo Hong Nam, Tran Thuy Uyen Phuong, Vo Lam Chuong, Truong Nguyen Luan Vu*
Faculty of Mechanical Engineering, Ho Chi Minh City University of Technology and Education, Ho Chi Minh City, Vietnam
*E-mail: vutnl@hcmute.edu.vn

Received: 11 January 2025 / Revised: 23 April 2025 / Accepted: 23 April 2025
Published online: 23 May 2025

Abstract. In the machining industry, the demands for precision and high speed of machine tools in CNC machines are increasingly high. The crucial component of these kinds of machines is a feed drive (FD) system, which comprises a servo motor coupled with a ball screw. Therefore, in this paper, a cascade scheme consisting of an inner and outer loop, which are also called the secondary and primary loops respectively, is suggested to control the feed drive system to improve the system's performance regarding tracking control and disturbance rejection. A filtered proportional integral (PI) controller is suggested for the secondary loop, and its tuning guidelines are established through the internal model control (IMC) approach. Additionally, a fractional-order proportional derivative (FOPD) controller and its design methodology in the frequency domain are introduced for the primary loop. The robust stability of the controlled system is assured by the maximum sensitivity function (M_s value). The investigation carried out through simulation focused on the feed drive system, and the findings indicated that the suggested control strategies fulfill the stringent criteria of a servo system.

Keywords: cascade control, CNC tool machines, feed drive systems, fractional-order controllers, internal model control.

1. INTRODUCTION

In order to control the position of the components of a machine tool, including the cutting tool and workpiece, a feed drive system is normally adopted. Therefore, the positioning precision and moving speed determine the quality and productivity of the system.

The feed drive comprises a sliding table on the guide and is translated linearly by a ball screw. The ball screw is normally connected directly to the servo motor or via a gearbox for high-powered machines. The speed and positioning precision of the machine tool are generally affected by the control algorithms, mechanical drives and guides, and sensors used in each feed drive [1]. The design of control algorithms for the feed drive system aims to enhance precision and reduce disturbances during machining, such as vibrations caused by the system itself or by changes in depth of cut and feed rate. Because the DC motor has excellent specifications in terms of speed and position control, it is usually used for feed drive systems in CNC machine tools [2].

In CNC machine tools, the feed drive controller typically has two control loops: a proportional (P) or proportional derivative (PD) controller is used for position control, and a proportional integral (PI) controller is utilized for velocity control [3, 4]. Consequently, the cascade structure with two closed loops—the outer loop, or primary controller, for position control and the inner loop, or secondary controller, for velocity control—is used for the feed drive system in this article. Actually, the controllers are still based on proportional integral derivative (PID) control with some modifications to achieve better performance of the controlled system.

The PID controller has been widely used in process industries, and due to its simple structure, it is easy to implement and shows high control performance, including good set-point tracking as well as good disturbance rejection. However, tuning the PID controller parameters becomes difficult if the system is unstable, has slow feedback, experiences vibrations, or fails to achieve the desired accuracy. Numerous experiments have been documented to increase the cascade system's control accuracy. Garrido and Díaz [5] proposed a method for adjusting the cascade system that uses the direct synthesis technique as the basis for the tuning rules, with the primary acting as the P controller and the secondary as the PI controller. Other researchers have proposed various methods for tuning both control loops of cascade systems or modifying the control structure by combining with a filter or the Smith predictor to enhance the system responses [6–8]. Unfortunately, most of the methods mentioned are not suitable for FD systems with high position control requirements.

In order to improve system performance to satisfy the high demands for a servo system, some researchers have suggested adopting nonlinear control techniques. In [9], a robust adaptive fuzzy compensation controller is proposed for a servo motor. A conventional P/PI controller is used for a cascade control scheme. However, the authors also used an adaptive fuzzy logic system to estimate friction. In [10], the authors use a linear model predictive control (MPC) and an adaptive MPC (AMPC) with an additional integral action to deal with model uncertainties. Those methods have been proven to

achieve better performance compared with other classical controllers. However, they are quite sophisticated to implement in real-time applications.

Recently, the generalization of the PID controller based on fractional calculus, which is called the fractional-order PID (FOPID) [11], has been introduced, in which two extra parameters in terms of the fractional orders of integral and derivative are included. Therefore, the main advantage of the FOPID controller is its flexibility in tuning control parameters, as well as greater robustness compared to the integer-order one. Many researchers have proposed using this controller in process control. However, it is commonly applied in single-input, single-output systems or multivariable processes, and rarely used in complex structures such as cascade systems. Yumuk et al. [6] suggested a parallel cascade approach using a PD controller for the primary loop and a FOPI controller for the secondary loop. Internal model control is utilized to derive the tuning rules. However, without a specific systematic methodology, the robust stability is only supported by simulation studies.

In this paper, a PI controller, whose tuning rules are based on the IMC structure, is adopted for the inner loop. For the outer loop, a fractional-order PD (FOPD) controller is proposed, and its design method is derived from the frequency domain [7,12]. The structure of this paper is as follows. In Section 2, a brief introduction to a mechanism system, including a mechanical system, a DC servo motor model, and a sliding table, is provided. In addition, the proposed PID controller for the inner loop and the fractional-order PD controller in the frequency domain are also mentioned. Section 3 refers to the design method for each control loop. Some criteria for evaluating the system's performance are addressed in Section 4. The simulation study and conclusion will be covered in Section 5 and Section 6, respectively.

2. SYSTEM DESCRIPTION

2.1. The mechanism structure

In general, the mechanism part of an FD system mainly comprises a servo motor, ball screw, linear encoder, and table as shown in Fig. 1.

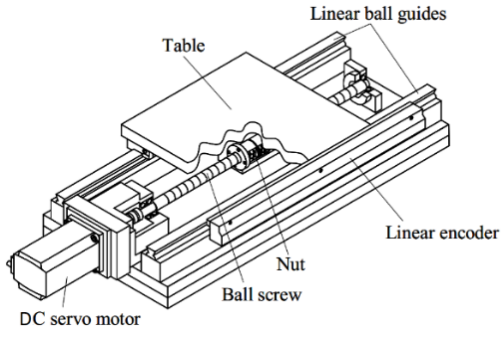

Fig. 1. Detailed view of a feed drive system [13,14]

2.2. Mathematical modeling

2.2.1. *The servo motor modeling*

In this paper, a DC servo motor is addressed, and its block diagram is also described as shown in Fig. 2.

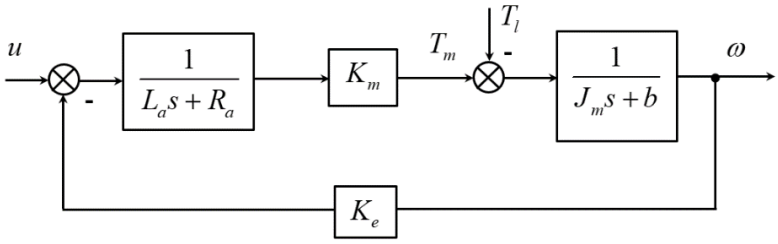

Fig. 2. Block diagram of a DC servo motor

Therefore, the mathematical model of the servo motor is derived as follows

$$G_1(s) = \frac{\omega(s)}{U(s)} = \frac{K_m}{(L_a s + R)(J_m s + b) + K_m K_e}, \tag{1}$$

where R_a is the armature resistance (Ohm); L_a is the armature inductance (H); K_m is the torque constant (Nm/A); K_e is the back EMF constant (V/rad/s); T_m is the torque of the motor (Nm); T_l is the torque of the load (Nm); J_m is the inertial moment of the motor shaft (kgm^2); u : is applied voltage to the motor (V); ω is the angular velocity of the motor shaft (rad/s).

$$G_1(s) = \frac{\omega(s)}{U(s)} = \frac{K}{(\tau_m s + 1)(\tau_e s + 1)}, \tag{2}$$

where K is the gain of the motor; τ_e and τ_m are the electrical and mechanical time constants, respectively; and normally, τ_m is much larger than τ_e ($\tau_m \gg \tau_e$).

2.2.2. *The ball screw modeling*

To improve the performance of the feed drive system, it is necessary to enhance the quality of the control system. First, the system's specifications, states, and modeling must be accurately analyzed. On that basis, the system controller can be designed.

Therefore, the feed drive system has been fully analyzed and modeled in many studies. The mechanical components in the system are modeled, and the general block diagram is shown in Fig. 3 [12].

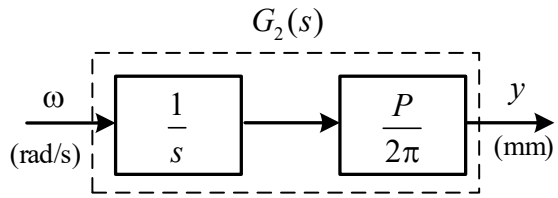

P is the lead of the ball screw (m), y is the position of the table (m)

Fig. 3. Block diagram of the ball screw

The mathematical model of the mechanical system is represented by the following equation

$$G_2(s) = \frac{Y(s)}{\omega(s)} = \frac{P}{2\pi s}. \tag{3}$$

2.3. The proposed control structure

2.3.1. *The cascade control scheme*

The control scheme of the feed drive system presented in this paper is a cascade control system consisting of two closed loops: the velocity control loop of the servo motor and the position control loop. Normally, both closed loops use classical controllers such as PI, P, and PD (Fig. 2). Based on the characteristics of this control structure, disturbances are attenuated more quickly and their effects are minimized before reaching the primary loop.

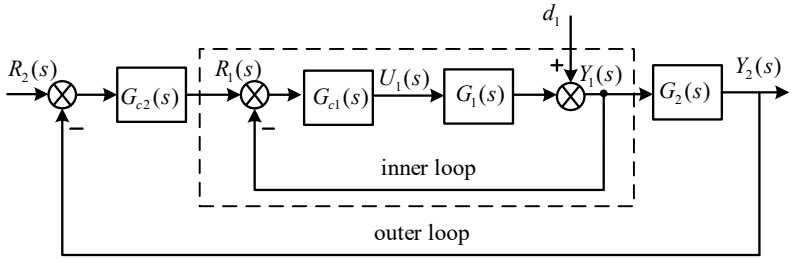

$G_1(s)$ is the transfer function of the servo motor, $G_{c1}(s)$ is the the inner loop controller, $G_2(s)$ is the transfer function of the mechanical system, $G_{c2}(s)$ is the outer loop controller, d_1 is a disturbance signal in the inner loop

Fig. 4. Block diagram of an FD system

From Fig. 4, the transfer functions of the inner and outer loops are given as follows

$$\frac{Y_1(s)}{R_1(s)} = \frac{G_{c1}(s)G_1(s)}{1 + G_{c1}(s)G_1(s)}, \tag{4}$$

$$\frac{Y_2(s)}{R_2(s)} = \frac{G_{c1}(s)G_1(s)G_{c2}(s)G_2(s)}{1 + G_{c1}(s)G_1(s) + G_{c1}(s)G_1(s)G_{c2}(s)G_2(s)}. \tag{5}$$

2.3.2. *PID controller for the secondary loop*

Normally, the PID controller has three parameters to tune, including the proportional gain (K_c), integral time (τ_I), and derivative time (τ_D). The transfer function of the PID controller is given as follows

$$G_{c1}(s) = K_c \left(1 + \frac{1}{\tau_I s} + \tau_D s\right) \frac{as + 1}{bs + 1}, \tag{6}$$

where a and b are the two constants of the filter.

2.3.3. *The FOPD controller in the frequency domain for the primary loop*

Fractional calculus is a generalization of ordinary calculus. Therefore, it gives the continuous transfer function of the FOPD controller as follows [12,15]

$$G_{c2}(s) = K_{p2} + K_{d2}s^{\alpha}, \quad (0 < \alpha \leq 1). \tag{7}$$

By substituting $s = j\omega$ into Eq. (7), the FOPD controller is presented in the frequency domain in Eq. (8)

$$G_{c2}(j\omega) = K_{p2} + K_{d2}(j\omega)^{\alpha}. \tag{8}$$

Expanding $(j\omega)^{\alpha}$ gives

$$(j\omega)^{\alpha} = \omega^{\alpha} j^{\alpha} = \omega^{\alpha}\left[e^{j\left[\frac{\pi}{2}+2n\pi\right]}\right]^{\alpha} = \omega^{\alpha}\left[e^{j\left[\frac{\pi}{2}\alpha+2n\alpha\pi\right]}\right], \tag{9}$$

where $n = 0, \pm\frac{1}{\alpha}, \pm\frac{2}{\alpha}, \ldots, \pm\frac{m}{\alpha}$. Finally, the following equation is derived

$$(j\omega)^{\alpha} = \omega^{\alpha}(\cos\gamma_d + j\sin\gamma_d), \quad \gamma_d = \frac{\pi\alpha}{2}. \tag{10}$$

A complex equation for the FOPD controller can be obtained by substituting Eq. (10) into Eq. (8) and rearranging

$$G_{c2}(j\omega) = \left(K_{p2} + K_{d2}\omega^{\alpha}\cos\gamma_d\right) + jK_{d2}\omega^{\alpha}\sin\gamma_d, \tag{11}$$

where $\gamma_d = \frac{\pi\alpha}{2}$.

3. METHODOLOGY

This study addresses the FOPD controller for the primary loop and proposes the IMC control strategy for the secondary loop. Thus, the proposed cascade control structure is modified as shown in Fig. 5, where the servo motor model is denoted by $\tilde{G}_1(s)$ and $q(s)$ is the IMC controller.

From Figs. 4 and 5, the relationship between the classical controller (G_{c1}) and the IMC controller (q) is given as follows

$$G_{c1}(s) = \frac{q(s)}{1 - \tilde{G}_1(s)q(s)}. \tag{12}$$

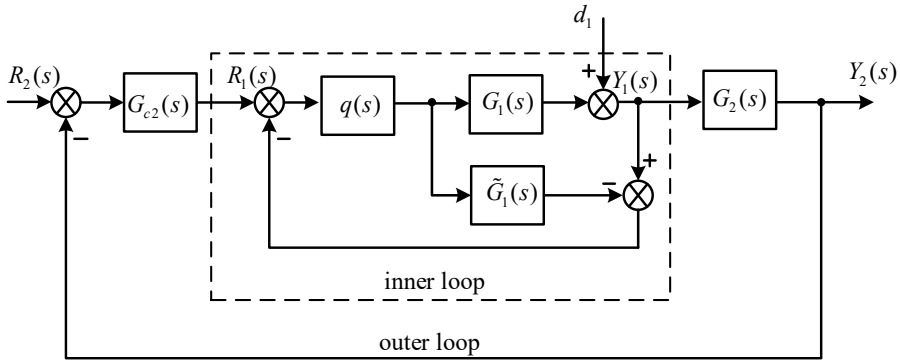

Fig. 5. The cascade scheme combined with the IMC structure for the inner loop

3.1. The inner controller design

Eq. (3) is analyzed into two components

$$G_1(s) = \tilde{G}_1(s) = p_m(s)\, p_a(s), \tag{13}$$

$$\begin{cases} p_m(s) = \dfrac{K}{(\tau_m s+1)(\tau_e s+1)}, \\ p_a(s) = 1, \end{cases} \tag{14}$$

$$\Rightarrow p_m^{-1} = \frac{(\tau_m s+1)(\tau_e s+1)}{K}. \tag{15}$$

The inner loop includes the servo motor transfer function Eq. (3) and the controller $G_{c1}(s)$. In this research, the controller is designed using the IMC structure mentioned above. The filter, in this case, can also be chosen as follows

$$q(s) = p_m^{-1}(s) f(s), \tag{16}$$

where

$$f(s) = \frac{\beta_1 s+1}{(\lambda_1 s+1)^2}. \tag{17}$$

By substituting Eqs. (13), (14) and (16) into Eq. (12), the ideal feedback controller is obtained as

$$G_{c1}(s) = \frac{(\tau_m s+1)(\tau_e s+1)(\beta_1 s+1)}{K\left[(\lambda_1 s+1)^2 - (\beta_1 s+1)\right]} = \frac{(\tau_m s+1)(\tau_e s+1)(\beta_1 s+1)}{Ks\left(\lambda_1^2 s + 2\lambda_1 - \beta_1\right)}. \tag{18}$$

Comparing the ideal controller Eq. (18) with the proposed PID controller Eq. (6), we can derive the analytical tuning guidelines for the PID controller as follows

$$\tau_I = \tau_m + \tau_e, \quad \tau_D = \frac{\tau_m \tau_e}{\tau_m + \tau_e}, \quad K_C = \frac{\tau_m + \tau_e}{K(2\lambda_1 - \beta_1)}, \tag{19}$$

$$a = \beta_1, \quad b = \frac{\lambda_1^2}{2\lambda_1 - \beta_1}. \tag{20}$$

There are two poles in the transfer function of the servo motor. Therefore, the value of β_1 is selected to cancel out the pole that is nearest to the imaginary axis ($s = -1/\tau_m$) to ensure a fast response as well as the robustness of the inner loop. By substituting $s = -1/\tau_m$ into the following equation and using Eq. (14), we obtain β_1 as follows

$$1 - G_1(s)q(s)|_{s=-1/\tau_m} = \left|1 - \frac{p_a(s)\,(\beta s + 1)}{(\lambda s + 1)^2}\right|_{s=-1/\tau_m} = 0, \tag{21}$$

$$\Rightarrow \beta_1 = \tau_m \left[1 - \left(1 - \frac{\lambda_1}{\tau_m}\right)^2\right]. \tag{22}$$

3.2. Outer loop design

Fig. 6 displays the block diagram of the outer loop where $\left(y_1/r_1\right)_d$ is the desired closed-loop transfer function of the secondary loop. Consequently, Eq. (23) describes the equivalent transfer function of the whole controlled system (from r_2 to y_2)

$$\frac{Y_2}{R_2} = \frac{G_{c_2}(s)\left(y_1/r_1\right)_d G_2(s)}{1 + G_{c_2}(s)\left(y_1/r_1\right)_d G_2(s)}. \tag{23}$$

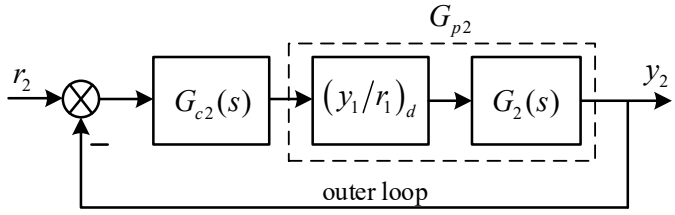

Fig. 6. The control structure design of the outer loop

From Fig. 6, the primary transfer function and the outer loop controller are derived as the following equations, Eq. (24) and Eq. (25), respectively

$$G_{p2}(s) = \left(y_1/r_1\right)_d G_2(s) = \frac{\beta s + 1}{(\lambda_2 s + 1)^2}\frac{K_2}{s}, \tag{24}$$

$$G_{c2} = \frac{1}{G_{p2}}\frac{\left(y_2/r_2\right)}{1 - \left(y_2/r_2\right)} \simeq \frac{1}{\tilde{G}_{p2}}\frac{\left(y_2/r_2\right)_d}{1 - \left(y_2/r_2\right)_d}. \tag{25}$$

Ideally, $\tilde{G}_{p2}(s) = G_{p2}(s) = \dfrac{\beta s + 1}{(\lambda_2 s + 1)^2}\dfrac{K_2}{s}$, and $\left(y_2/r_2\right)_d$ is the desired response of the outer loop. In this case, it is chosen as in Eq. (26) to guarantee the strict requirements of a servo system.

$$\left(\frac{y_2}{r_2}\right)_d = \frac{1}{\lambda_2 s + 1}, \tag{26}$$

where λ_2 is the desired response time of the outer-loop control system.

By substituting Eq. (26) and $\tilde{G}_{p2}$ into Eq. (25), the primary controller is obtained

$$G_{c2} = \frac{s(\lambda_1 s + 1)^2}{K_2(\beta s + 1)} \frac{1}{\lambda_2 s} = \frac{(\lambda_1 s + 1)^2}{K_2 \lambda_2 (\beta s + 1)}. \tag{27}$$

Substituting $s = j\omega$ to convert G_{c2} into the frequency domain in complex form, we have

$$G_{c2} = \frac{1 + 2\beta\lambda\omega^2 - \lambda^2\omega^2}{K_2\lambda_2(1 + \beta^2\omega^2)} + j\frac{\omega(2\lambda - \beta + \beta\lambda^2\omega^2)}{K_2\lambda_2(1 + \beta^2\omega^2)}. \tag{28}$$

Comparing Eq. (28) and Eq. (11), the tuning rules of the outer loop controller are obtained as

$$K_{d2} = \frac{1}{\omega^\alpha \sin\gamma_d} \frac{\omega(2\lambda - \beta + \beta\lambda^2\omega^2)}{K_2\lambda_2(1 + \beta^2\omega^2)}, \tag{29}$$

$$K_{p2} = \frac{1 - \lambda^2\omega^2 + 2\beta\lambda\omega^2}{K_2\lambda_2(1 + \beta^2\omega^2)} - \frac{\cos\gamma_d}{\sin\gamma_d} \frac{(2\lambda - \beta + \beta\lambda^2\omega^2)\omega}{K_2\lambda_2(1 + \beta^2\omega^2)}. \tag{30}$$

Note that the value of ω will be chosen to guarantee the robustness of the controlled system based on the maximum sensitivity function, which is described in the next section.

4. PERFORMANCE AND ROBUSTNESS MEASUREMENTS

4.1. Performance indices

4.1.1. *Overshoot*

Overshoot is a performance index that evaluates the peak of the response after a step change in set-point or disturbance. Normally, it is calculated as a percentage.

4.1.2. *Integral absolute error (IAE)*

The IAE criterion is used to evaluate the closed-loop performance for disturbance rejection as well as set-point tracking. It is defined as

$$IAE = \int_0^\infty |e(t)| \mathrm{d}t. \tag{31}$$

4.1.3. *Total variation (TV)*

TV is a good measure of the signal's smoothness. It describes the total variation of the manipulated variable. It is calculated by the following equation

$$TV = \sum_{i=1}^{\infty} |u_{i+1} - u_i|. \tag{32}$$

In a control system, this index should also be as small as possible.

4.2. Robust stability

Normally, the maximum sensitivity function, which is defined in Eq. (34), is used to verify the robust stability of a feedback control loop

$$M_s = \max_{\omega} |S(j\omega)|, \tag{33}$$

where $S = (1 + L)^{-1}$, and L is an open-loop transfer function of the controlled system. Typically, $|S|$ is small at lower frequencies and approaches 1 at higher frequencies. However, at certain specific frequencies, a peak value of M_s can be larger than 1 which deteriorates the system performance [12]. Consequently, the peak value of M_s is generally utilized to assess the robustness of the controlled system concerning both robust stability and system performance. According to Skogestad and Postlethwaite [16], the value of M_s should ideally be close to 1. Therefore, in this work, the value of frequency ω is selected based on maintaining this value close to 1.

5. SIMULATION STUDY

To demonstrate the effectiveness of the proposed method above, we consider the following case: the parameters of a DC servo motor and a lead ball screw are given in Table 1.

Table 1. Parameters of the DC servo motor and lead ball screw [12]

Parameters	Description	Values
L_a	Armature inductance	8×10^{-5} (H)
R_a	Armature resistance	0.316 (Ohm)
J_m	Torque developed by the motor	1.34×10^{-5} (kg.m^2)
B	Viscous friction constant of motor and load	1.82×10^{-5} (Nm/rad/s)
K_m	Torque constant	0.03 (Nm/A)
K_e	Back EMF constant	0.03 (V/rad/s)
P	Pitch of ball screw	0.01 (m)

From the above parameters and Eqs. (1) and (2), we derive the transfer function of the servo motor

$$G_1(s) = \frac{\omega(s)}{U(s)} = \frac{33.1217}{(0.0464s+1)(0.00039544s+1)}. \tag{34}$$

For the inner loop, the adjustable parameter λ is chosen as $\lambda = 0.01$. Therefore, from Eqs. (20) and (21), the control parameters of the inner loop are obtained as

$$\beta_1 = 0.0178, \quad K_{c1} = 0.6557, \quad \tau_I = 0.0468, \quad \tau_D = 3.92 \times 10^{-4}, \quad a = 0.0178, \quad b = 0.0464.$$

For the primary loop, the fractional order is chosen to be less than 1 due to the over-damped characteristic of the controlled system. Fig. 7 illustrates the position responses for $\alpha = 0.7$, $\alpha = 0.8$, and $\alpha = 0.9$, respectively. From the figure, it can be seen that the larger the value of α, the faster the response of the controlled system. In this work, α is chosen as 0.8 to guarantee both the system response and the robustness of the system. Then, the frequency ω is chosen to keep the M_s value close to 1. In this case, $\omega = 100$ and $M_s = 1.057$. According to Eqs. (29) and (30), the outer loop controller is derived as

$$G_{c2}(s) = 43833 + 793.167s^{0.8}. \tag{35}$$

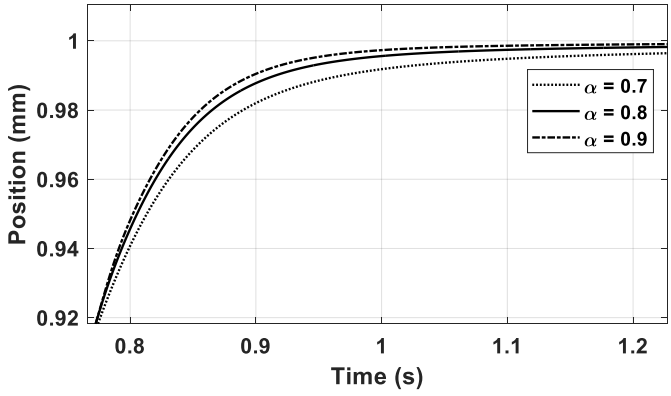

Fig. 7. The position response with various values of α

The suggested approach and the traditional PD/PID controller [17] for the cascade system are contrasted in this study. Table 2 lists the controllers' parameters as well as the performance metrics of the suggested approach, such as overshoot, absolute error, and total variation (TV).

Figs. 8 and 9 display the closed-loop responses for the outer loop (position) and the inner loop (velocity), respectively. It is clear from these figures that the tracking control fully satisfies the stringent requirements for the feed drive system, achieving a quick

Table 2. The controller parameters and the performance indices

	Inner loop	Outer loop
Proposed (FOPD/PID)	$G_{c1}(s) = 0.6557\left(1 + \frac{1}{0.0468s} + 0.000392s\right)\frac{0.0178s+1}{0.0464s+1}$	$G_{c_2}(s) = 43833 + 793.167s^{0.8}$
PD/PID	$G_{c1}(s) = 1.7649\left(1 + \frac{1}{0.0047s} + 0.000253s\right)\frac{1}{0.00002s+1}$	$G_{c_2}(s) = 3927000 + 157.079s$
TV	0.9999	
IAE	0.4453	
Overshoot	0 (%)	

response and no overshoot in both methodologies. However, in Fig. 9, the velocity response of the PD/PID method exhibits oscillations at the target position. The control signals are presented in Fig. 10 to demonstrate that the proposed method yields a relatively smooth control signal, remaining within the rated voltage limit (24 V) of the servo motor. Additionally, the control signal from the proposed method is contrasted with that of the classical controllers. Fig. 11 shows that the control signal from the classical method experiences high-frequency oscillations to maintain an equivalent position response to that of the proposed method.

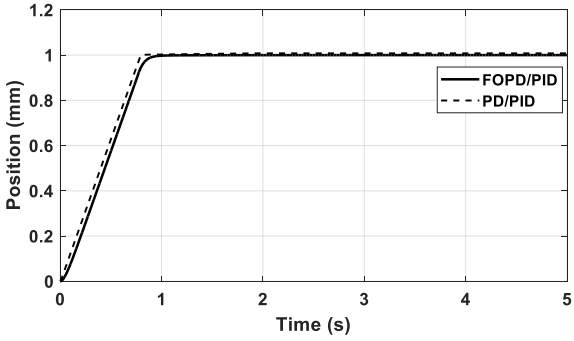

Fig. 8. The position response of the feed drive system

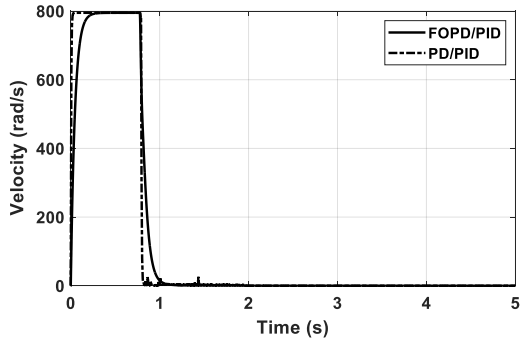

Fig. 9. The velocity response of the inner loop

Fig. 12 illustrates the movement of the sliding table in both directions. It is obvious that the forward and backward movements still guarantee the requirements of the servo system in terms of fast response and no overshoot at the target position. However, the proposed method still has a restriction regarding the choice of the fractional order value. Its value is obtained through simulation without being analytically proven.

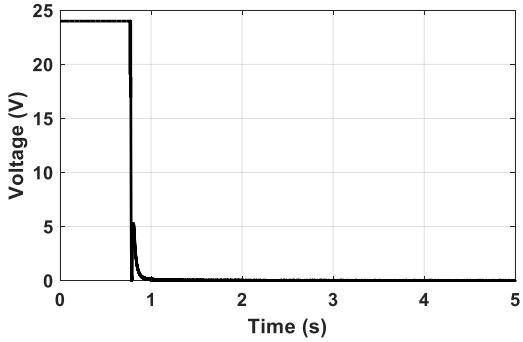

Fig. 10. The control voltage of the fractional-order controller

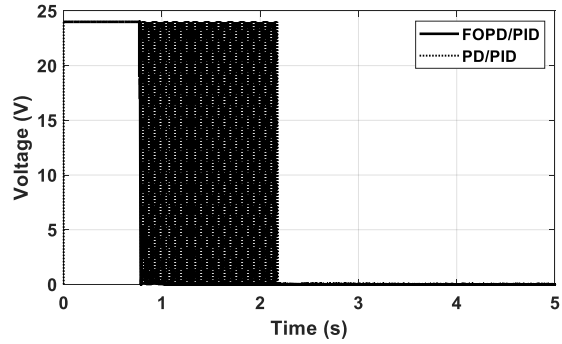

Fig. 11. The control voltages in two cases

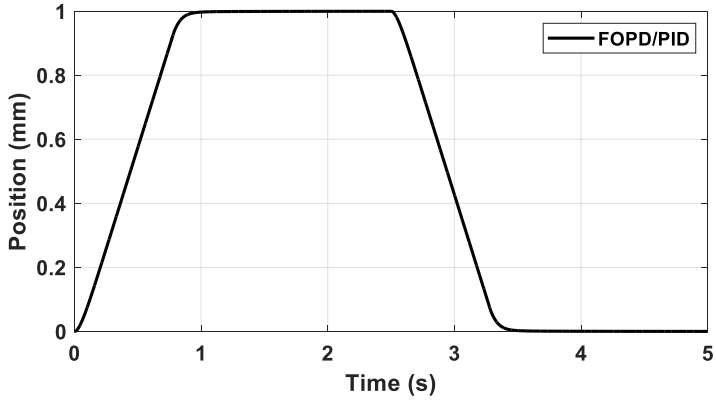

Fig. 12. The movement of the sliding table in both directions

6. CONCLUSION

In this study, a cascade control architecture consisting of two control loops is proposed for the feed drive system. The inner loop is responsible for controlling velocity, while the outer loop manages position. A PID controller equipped with a filter is recommended for the inner loop, and a FOPD controller is suggested for the outer loop. The tuning guidelines for the inner controller are derived from the widely recognized IMC framework, while the outer controller is formulated in the frequency domain, with the frequency coefficient selected to guarantee the robustness of the controlled system. Furthermore, during the design of both control loops, the desired response times are determined to satisfy the stringent demands of the feed drive system's position control. The results from simulations indicate that the proposed methods deliver impressive position tracking with a quick response time and no overshoot.

DECLARATION OF COMPETING INTEREST

The authors declare that they have no known competing financial interests or personal relationships that could have appeared to influence the work reported in this paper.

FUNDING

This research received no specific grant from any funding agency in the public, commercial, or not-for-profit sectors.

REFERENCES

[1] Y. Altintas, A. Verl, C. Brecher, L. Uriarte, and G. Pritschow. Machine tool feed drives. *CIRP Annals*, **60**, (2), (2011), pp. 779–796. https://doi.org/10.1016/j.cirp.2011.05.010.

[2] S. Tiwari, A. Bhatt, A. C. Unni, J. G. Singh, and W. Ongsakul. Control of DC motor using genetic algorithm based PID controller. In *2018 International Conference and Utility Exhibition on Green Energy for Sustainable Development (ICUE)*, IEEE, (2018), pp. 1–6. https://doi.org/10.23919/icue-gesd.2018.8635662.

[3] S.-H. Suh, S. K. Kang, D.-H. Chung, and I. Stroud. *Theory and design of CNC systems*. Springer Science & Business Media, (2008).

[4] Z. Sun, G. Pritschow, P. Zahn, and A. Lechler. A novel cascade control principle for feed drives of machine tools. *CIRP Annals*, **67**, (1), (2018), pp. 389–392. https://doi.org/10.1016/j.cirp.2018.03.004.

[5] R. Garrido and A. Díaz. Cascade closed-loop control of solar trackers applied to HCPV systems. *Renewable Energy*, **97**, (2016), pp. 689–696. https://doi.org/10.1016/j.renene.2016.06.022.

[6] E. Yumuk, M. Güzelkaya, and İ. Eksin. Analytical fractional PID controller design based on Bode's ideal transfer function plus time delay. *ISA Transactions*, **91**, (2019), pp. 196–206. https://doi.org/10.1016/j.isatra.2019.01.034.

[7] T. N. L. Vu, V. L. Chuong, N. T. N. Truong, and J. H. Jung. Analytical design of fractional-order PI controller for parallel cascade control systems. *Applied Sciences*, **12**, (2022). https://doi.org/10.3390/app12042222.

[8] M. A. Siddiqui. Design of parallel cascade controller for nonlinear continuous stirred tank reactor. *Scientific Reports*, **15**, (2025). https://doi.org/10.1038/s41598-025-89455-6.

[9] Y. Liu, Z. Z. Wang, Y. F. Wang, D. H. Wang, and J. F. Xu. Cascade tracking control of servo motor with robust adaptive fuzzy compensation. *Information Sciences*, **569**, (2021), pp. 450–468. https://doi.org/10.1016/j.ins.2021.03.065.

[10] V. Leipe, C. Hinze, A. Lechler, and A. Verl. Model predictive control for compliant feed drives with offset-free tracking behavior. *Production Engineering*, **17**, (2023), pp. 805–814. https://doi.org/10.1007/s11740-023-01206-6.

[11] S. Jayaram and N. Venkatesan. Design and implementation of the fractional-order controllers for a real-time nonlinear process using the AGTM optimization technique. *Scientific Reports*, **14**, (2024). https://doi.org/10.1038/s41598-024-82258-1.

[12] V. L. Chuong, N. H. Nam, L. H. Giang, and T. N. L. Vu. Robust fractional-order PI/PD controllers for a cascade control structure of servo systems. *Fractal and Fractional*, **8**, (2024). https://doi.org/10.3390/fractalfract8040244.

[13] R. Sato and M. Tsutsumi. Mathematical model of feed drive systems consisting of AC servo motor and linear ball guide. *Journal of the Japan Society for Precision Engineering, Contributed Papers*, **71**, (5), (2005), pp. 633–638. https://doi.org/10.2493/jspe.71.633.

[14] R. Sato and M. Tsutsumi. Modeling and controller tuning techniques for feed drive systems. In *Dynamic Systems and Control, Parts A and B*, ASMEDC, IMECE2005, (2005), pp. 669–679. https://doi.org/10.1115/imece2005-80596.

[15] T. N. L. Vu and M. Lee. Analytical design of fractional-order proportional-integral controllers for time-delay processes. *ISA Transactions*, **52**, (2013), pp. 583–591. https://doi.org/10.1016/j.isatra.2013.06.003.

[16] S. Skogestad and I. Postlethwaite. *Multivariable feedback control: analysis and design*. John Wiley & Sons, 2nd edition, (2001).

[17] N. H. Nam, T. N. L. Vu, and V. L. Chuong. PID controller tuning rules for feed drive systems. In *2024 7th International Conference on Green Technology and Sustainable Development (GTSD)*, IEEE, (2024), pp. 159–164. https://doi.org/10.1109/gtsd62346.2024.10675245.